www.MaterialsViews.com

Photonic Crystal Hydrogel Enhanced Plasmonic Staining for Multiplexed Protein Analysis

Zhongde Mu, Xiangwei Zhao, Yin Huang, Meng Lu,* and Zhongze Gu**

Plasmonic nanoparticles are commonly used as optical transducers in sensing applications. The optical signals resulting from the interaction of analytes and plamsonic nanoparticles are influenced by surrounding physical structures where the nanoparticles are located. This paper proposes inverse opal photonic crystal hydrogel as 3D structure to improve Raman signals from plasmonic staining. By hybridization of the plasmonic nanoparticles and photonic crystal, surface-enhanced Raman spectroscopy (SERS) analysis of multiplexed protein is realized. It benefits the Raman analysis by providing high-density "hot spots" in 3D and extra enhancement of local electromagnetic field at the band edge of PhC with periodic refractive index distribution. The strong interaction of light and the hybrid 3D nanostructure offers new insights into plasmonic nanoparticle applications and biosensor design.

1. Introduction

Benefited by the localized surface plasmon resonance (LSPR) effect, metal nanoparticles have been exploited for biomolecule sensing applications in the fields of biological science,[1–4] biomedical research,[5,6] clinic diagnostics, and food safety monitoring.[7,8] The interaction of LSPR modes with target biomolecules results in quantitative changes of optical signals and thus the metal nanoparticles are also called plasmonic nanoparticles, which offer the colorimetric and label-free analysis of biomolecules. Meanwhile, the plasmonic nanoparticles are also utilized to significantly improve the fluorescence and Raman spectroscopies.[9–11] Through means of staining, the nanoparticles can interact with analytes in a controllable and facile way, based on which various sensitive and flexible analytical methods have been developed. For instance, the silver staining process in gel electrophoresis and histological characterization, through the in situ reduction of silver nitrate, can visualize protein and DNA molecules via colorimetric signals generated by the LSPR.[12–14] Mirkin's group used silver staining to enhance signal of the Raman tags on gold nanoparticles for multiplexed biomolecule detection.[15,16] Recently Li et al. stained the surface of fresh citrus fruits with gold nanoparticles in ultrathin silica or alumina shells for the identification of pesticide residues by surface-enhanced Raman spectroscopy (SERS).[17]

The colorimetric, fluorescent, and Raman scattering signal generated by the plasmonic staining can be modulated by the surrounding physical structures especially when these structures are ordered and periodic in nanoscale equivalent to the wavelength, the so called photonic crystal (PhC). Since the manipulation of local density of states by PhC structures can improve the light-matter interactions, enhanced fluorescence detections using PhC and plasmonic hybrids have been implemented to improve the limit of detection for many fluorescence-based assays. The PhC structure also has great potentials to increase the interaction of light and plasmonic nanoparticles and consequently generate stronger optical outputs. Cunningham's group combined a planar 2D PhC substrate and metal nanorods and demonstrated enhanced SERS signal from organic compounds.[18] For practical applications, it is highly desirable to hybridize plasmonic

Z. Mu, Prof. X. Zhao, Prof. Z. Gu
State Key Laboratory of Bioelectronics
School of Biological Science and Medical Engineering
Southeast University
Nanjing 210096, P. R. China
E-mail: xwzhao@seu.edu.cn; gu@seu.edu.cn
Y. Huang, Prof. M. Lu
Department of Electrical and Computer Engineering
Department of Mechanical Engineering
Iowa State University
Ames, IA 50011, USA
E-mail: menglu@iastate.edu

DOI: 10.1002/smll.201501829

small NANO MICRO

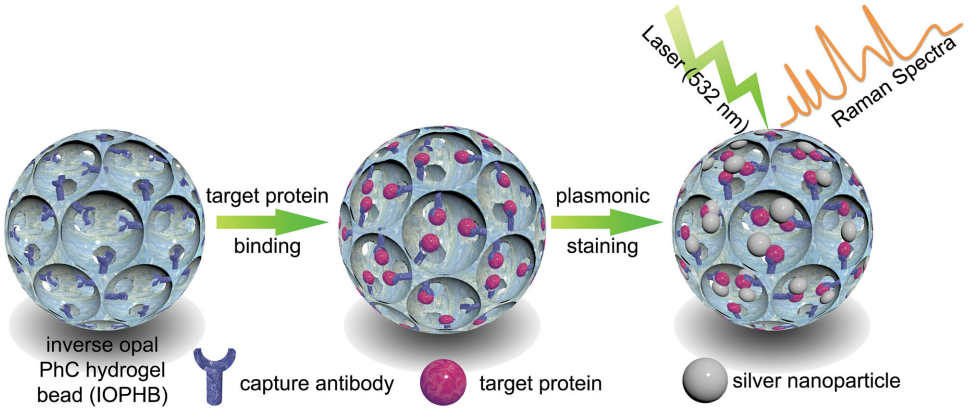

Figure 1. Schematic diagram of photonic-plasmonic hybrid IOPHB for multiplexed analysis of proteins by their Raman fingerprints. IOPHBs were fabricated using self-assembled silica photonic crystal beads (PCBs) as templates.

nanoparticles with PhC in a 3D space as 3D structure could support more hotspots and enable higher capture capacity for analytes. Unlike the 2D sensors fabricated on flat substrates, the integration of PhC and plasmonic nanoparticles in 3D is also challenging and significant for the wide applications of plasmonic staining.

Therefore, in this paper, we exploited plasmonic staining of an inverse opal PhC structure composed of polyacrylamide (PAM) hydrogel, a common electrophoresis medium for protein and DNA analysis, for multiplexed protein detection. As illustrated in **Figure 1**, the inverse optical PhC structure was molded into PAM hydrogel with highly ordered nanovoids and fabricated into microbeads with diameter of 200 μm. The inner surfaces of the nanovoids were modified with antibodies specific to target proteins and then exposed to analytes. After the capture of target molecules, the 3D PhC hydrogel was stained using plasmonic silver nanoparticles in order to create near field "hot spots" for the subsequent Raman scattering measurements.

This paper reports the design, fabrication, and characterization of the inverse opal PhC hydrogel beads (IOPHB) for enhanced 3D plasmonic staining. The PhC structure was theoretically analyzed using electromagnetic simulation in order to achieve the strong near field strength in the nanovoids. We optimized the staining process and Raman measurement conditions to maximize signal-to-noise ratio (SNR) and minimize relative standard deviation (RSD). A mixture of three heme proteins was analyzed using the photonic-plasmonic material in a multiplexed fashion.

2. Results and Discussion

2.1. IOPHB Fabrication

In this paper, PhC hydrogel was fabricated in form of bead rather than film throughout the experiments. The reason is that beads can be mixed with the solutions thoroughly by vortex or shaking which greatly facilitate the reaction, staining, and rinsing process. The IOPHB were inexpensively fabricated using self-assembled silica photonic crystal beads (PCBs) as the template. While PCBs were immerged in PAM pregel solution, the solution was infiltrated into voids of silica nanoparticles. After being cured with UV light, the pregel solution polymerized into a bulk periodic hydrogel network imbedded with the PCBs. The PAM hydrogel network will shrink and swell when exposed to anhydrous ethanol and double distilled water at 4 and 60 °C, respectively. Due to the different expansion coefficient of silica and PAM, the PCBs were easily peeled away from the bulk hydrogel after several circles of shrinkage and swelling. Finally, silica templates were removed by a soak using 1% hydrofluoric acid (HF) solution to obtain IOPHBs. By using different diameters of silica nanoparticles, the IOPHBs with controllable reflection peaks were achieved. As is shown in Figure S1 (Supporting Information), antibodies were immobilized in the network of the glutaraldehyde conjugated PAM hydrogel by the Schiff base reaction. After the subsequent antibody–antigen binding and silver staining, IOPHB were ready for label-free and multiplexed protein analysis.

2.2. Plasmonic Staining for IOPHB

PhC could enhance the SERS effect of plasmonic nanoparticles through "band edge" effect.[19] However, plasmonic nanoparticles may also change the position of photonic bandgap of PhC or its reflection peak when they are hybridized. Therefore, the process of combining the plasmonic nanoparticles and the IOPHB should be optimized to maximize the enhancement of Raman signals. In our experiment, different plasmonic staining times were tested to minimize the effect of plasmonic nanoparticles on PhC (inset in **Figure 2**a) by antibody modified IOPHB. We found that silver staining showed negligible effects on the reflection peak of IOPHB if the silver staining time was less than 15 min. Taking IOPHB with reflection peak at 650 nm as an example, the peak shifts were less than 1–2 nm (Figure 2a). However, the reflection peak blueshifted for 10 nm when time of staining was extended to 3.5 h (insets in Figure 2a). The change of reflection peak was due to change of effective refractive index in the nanovoids as more and more silver nanoparticles with negative refractive index loaded inside. It can also be seen that a hill-like peak emerged at 425 nm when time of silver

www.MaterialsViews.com

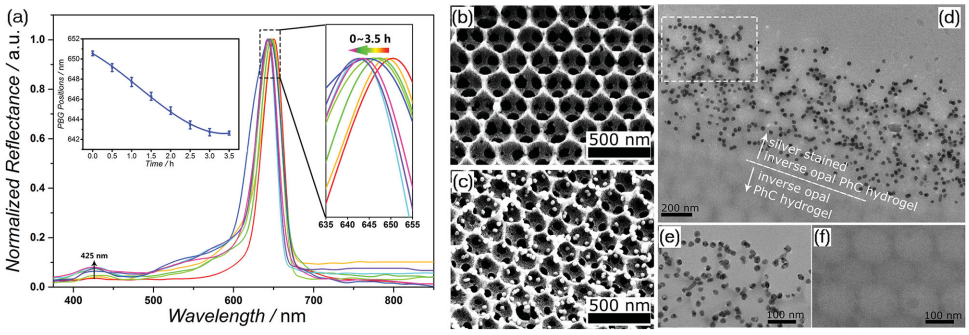

Figure 2. Reflection spectra and structure of silver stained IOPHB with reflection peak at 650 nm. a) Reflection spectra of IOPHB with different silver staining time. Left inset indicates the relationship of staining time and peak shift. Right inset is the magnification of reflection peaks. SEM images of the IOPHB surface before b) and after c) silver staining for 15 min. d) TEM image of cross sections of silver stained IOPHB. e) The enlarged area of the dashed rectangle in (d). f) The nonstained area of IOPHB.

staining was extended to more than 1 h. Since the diameter of the silver nanoparticles are 30 nm with LSPR located at 420 nm (Figure S2, Supporting Information), this peak indicated the amount of silver nanoparticles are relative high and aggregations of nanoparticles occurred. Therefore, in the sensing experiments the staining time was fixed at 15 min, which almost will not affect the band gaps of IOPHB but still guarantee sufficient amount of plasmonic nanoparticles for highly sensitive SERS signal generation. Scanning electron microscope (SEM) image of IOPHB after silver staining for 15 min is shown in Figure 2c. It can be seen that nanovoids of the IOPHB have the same hexagonal close packing alignments as silica nanoparticles in PCBs (Figure S3, Supporting Information). Besides, these nanovoids interconnected and extended to the inside of the hydrogel. This structure can provide not only large surface area for antibody immobilization but also high capacity for antibody–antigen binding.

As shown in Figure 2d, silver nanoparticles infiltrated about 1 μm deep into the IOPHB and formed contours of inverse opal structure. This was verified by more transmission electron microscopy (TEM) images captured from different positions of the silver stained IOPHBs in Figure S4c–f (Supporting Information), which also demonstrated the advantages of beads in staining. There is a clear boundary (white dashed line in Figure 2d) between silver stained region and unstained region. It also can be seen that the silver nanoparticles residue inside nanovoids rather than inside the hydrogel backbone. As the PAM hydrogel replicated face-center-cubic structure of the PCBs (Figure S3, Supporting Information), a periodic silver nanoparticle pattern in several-hundred-nanometer scale was formed with the highly ordered PhC hydrogel as the 3D skeleton. In contrast, there is only a ≈200 nm silver nanoparticles layer formed for silver stained nonporous hydrogel (Figure S4a, Supporting Information) and in which AgNPs distributed in a random pattern. Furthermore, the densities of AgNPs were also compared between silver stained nonporous hydrogel and PhC hydrogel (Figure S4b, Supporting Information). It can be seen that there is an increment of about 29.5% from nonporous hydrogel to PhC with reflection peak at 650 nm. This can be attributed to the high surface-to-volume ratio of the IOPHB.

2.3. Evaluation of Exciting Wavelengths

In order to couple the plamsonic particles and PhC structure for SERS, the relationship between the position of the excitation wavelength and reflection peaks of IOPHB was investigated. Taking the detection of myoglobin (Mb) as an example, three commonly used Raman excitation lasers, with emission wavelengths at 532, 633, and 785 nm, were employed to excite the SERS signal of plasmonic stained Mb in IOPHB with different reflection peaks centered at 540, 600, and 650 nm, respectively (**Figure 3**d). Figure 3a–c are the optical images of the IOPHBs taken by a microscope. Figure 3e–g is the SERS spectra collected from the three kinds of IOPHB. It could be seen that feature peaks of Mb could be obtained by the 532 nm laser for all three IOPHBs. Vibrational absorption signatures were given in Table S2 (Supporting Information). However, almost no discernable peaks were obtained by the 785 nm laser on any IOPHB and the 633 nm laser worked only on IOPHB with reflection peak of 600 nm. In addition, the high SERS intensities were obtained on IOPHB with reflection peak of 600 nm. The mechanism behind the phenomenon can be interpreted as follows. First, the Raman intensity is proportional to the fourth power of the excitation frequency $(1/\lambda)$[20] and excitation wavelength of 532 nm is closest to the LSPR peak of silver nanoparticles (420 nm). Thus, 532 nm was the best excitation wavelength for silver staining and strongest intensities of SERS were obtained for all three PhC hydrogels. Second, it has been found that the band edge of photonic bandgap (PBG) could induce reduced group velocity and consequently lead to large light matter interaction and enhancement of density of electromagnetic modes.[19] For reflection peak of 600 nm, excitation wavelength of 532 and 633 nm located at the two band edges of the band gap. Therefore, SERS intensities from the silver stained IOPHB with reflection peak of 600 nm were the highest. Furthermore, according to electromagnetic variational theorem of photonic crystal, power of lower frequencies tend to locate in high dielectric or high index region.[21] Consequently, electromagnetic field at 633 and 785 nm are likely to concentrate in hydrogel region and power of 532 nm distributes in the nanovoids. From the images of silver stained IOPHB it can be seen that most of the silver nanoparticles were locked inside

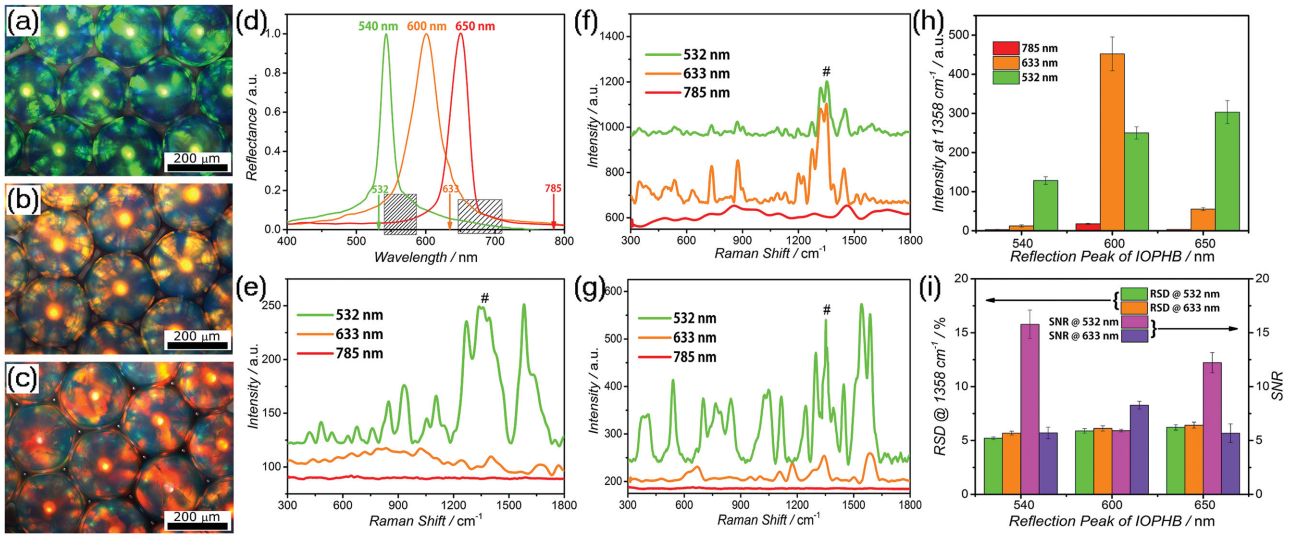

Figure 3. SERS analysis on three kinds of IOPHB. a–c) Images of the three kinds of IOPHB. d) Reflection spectra of three kinds of plasmonic stained IOPHB. The rectangle boxes beside 532 and 633 nm indicate the Raman scattering range from 300 to 1800 cm^{-1}. e–g) Raman spectra of 2.73×10^{-3} M Mb excited by 532, 633, and 785 nm laser on IOPHB with reflection peaks at 540, 600, and 650 nm, respectively. h) Relative Raman intensity (absolute value subtracted by baseline) at 1358 cm^{-1} on three kinds of IOPHBs (five data averaged). i) RSD and SNR of Raman signal on three IOPHBs (each calculated on twenty data).

the nanovoids of the inverse opal structure and most of the proteins were also distributed on the surface layer of inverse opal structure rather than inside the cross-linked skeleton of the hydrogel.[22,23] Consequently, the large fraction of 532 nm power concentrated inside the nanovoids could readily couple with LSPR band of the aggregated silver nanoparticles and enhanced the Raman signal most effectively.

Another issue worth considering is that the background Raman signals were also enhanced besides protein Mb. Therefore, SERS performances were evaluated by relative SERS intensities, RSD and SNR for choosing one kind of IOPHB with an appropriate reflection peak. Relative SERS intensities at 1358 cm^{-1}, which attributed to C—H stretching,[24,25] were calculated by the absolute values minus baseline and summarized in Figure 3h. The statistical data of RSD and SNR are shown in Figure 3i. It can be seen that, IOPHB with reflection peak at 600 nm excited by 633 nm laser yielded the highest SERS intensity. However, SNR at this wavelength is the lowest when compared with the other two IOPHB excited by 532 nm laser. Although IOPHB with reflection peak at 540 nm excited by 532 nm laser had the highest SNR, SERS intensity at this wavelength is smaller than the other two IOPHB. RSD of all these three IOPHB are about 5%, which means that reproducibility of the plasmonic staining is very good. In conclusion, taking both SERS intensity and SNR into consideration, IOPHB with reflection peak at 650 nm excited by 532 nm laser were chosen as the basic SERS measurement parameters for the following analysis.

2.4. Numerical Simulation

In order to understand the interaction of excitation light and the silver stained inverse opal structure, a finite difference time domain-based electromagnetic (EM) simulation tool (FDTD Solution, Lumerical Inc.) was used to model the local field distributions in the IOPHB with plasmonic nanoparticles. The model in the simulation is the counterpart of the IOPHB with reflection peak at 650 nm with silver staining time of 15 min. **Figure 4**a–c shows the normalized electric field distributions for the inverse opal hydrogel without silver nanoparticles when the structure is illuminated at 532, 633, and 785 nm, respectively. The normalization was calculated by using the electric field of the incident light as the reference. It can be seen from the figures that the electromagnetic fields are redistributed inside the nanovoids and exhibits energy hotspots near the hydrogel backbone. The positions of the energy hotspot vary depending on the wavelength of interest. This phenomenon is particularly favorable for SERS detection of proteins because the target protein molecules and the associated silver nanoparticles are anchored to the surface of the hydrogel backbone. The energy hotspots inside the ovals can enhance the localized surface plasmon resonances supported by the silver nanoparticles and result in a strong SERS effect.

To demonstrate how the ordered hydrogel interacts with the silver nanoparticles, the near field profiles of $|E/E_{inc}|$ near the silver nanoparticles were calculated for two different scenarios: silver nanoparticles without the hydrogel (Figure 4d–f) and silver nanoparticles with the PhC hydrogel (Figure 4g–i). Due to the LSPR effect, the amplitude of the electric field near nanoparticles (diameter of 30 nm) exhibits an approximately sixfold enhancement (36× for the intensity), referenced to the incident field at 532 nm. At 633 and 785 nm, the enhancement effect is less pronounced. The slightly high enhancement factor associated with the short wavelength excitation is because the excitation wavelength (532 nm) is close to the LSPR resonant wavelength shown in the UV–vis absorption spectrum (Figure S2, Supporting Information) of silver nanoparticles. When the PhC and the silver nanopar-

www.MaterialsViews.com

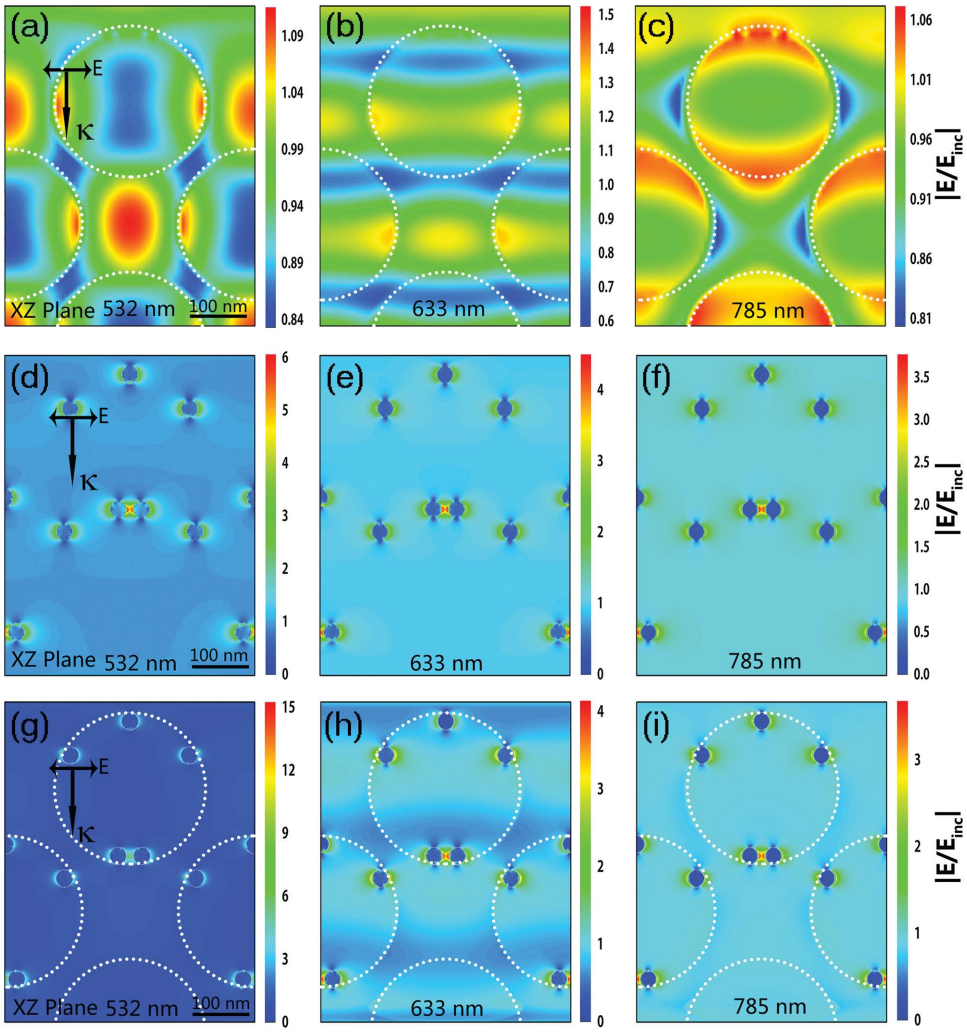

Figure 4. Simulated comparison among IOPHB, silver nanoparticals, and hybrid structure. $|E/E_{inc}|$ profiles in IOPHB, silver nanoparticles, and hybrid structure were plotted in images (a–c), (d–f), and (g–i), respectively. Color bars denoted the absolute ratio value between induced (E) and incident electric field (E_{inc}). White dash circles were the contours of nanovoids.

ticles are coupled, the field enhancement capability of the plasmon-coupled PhC structure is wavelength dependent. For example, at 633 and 785 nm, electric field enhancements ($|E/E_{inc}|$) are similar to the simulations with (Figure 4e,h) and without PhC (Figure 4f,i). At 532 nm, the energy hotspots near the hydrogel surface overlap the hotspots that formed adjacent to silver nanoparticles and in gaps between silver nanoparticle dimers. Positions of these hotspots were ideal for protein detection because the protein molecules are anchored to the hydrogel backbone and swinging inside the nanovoids.[22,23] At 532 nm, silver nanoparticle decorated PhC is capable of raising the local electric field by a factor of 15 compared to the incident field. It is worthwhile to note that the PhC offers an extra nine times enhancement compared to the silver nanoparticles without the PhC. In addition, the lack of hydrogel backbone will result in a random distribution and aggregations of silver nanoparticles, which deteriorate the quality of SERS. The extra enhancement could be associated with three possible reasons. First, the 532 nm resides closely to the peak of the UV–vis absorption spectrum of the silver nanoparticles and thus results in a strong LSPR effect. Second, PhC functions as a 3D matrix with highly ordered nanocavities that regulates the distribution of the stained nanoparticles. Finally, the PhC itself redistributed the electromagnetic field and offers energy hotspots. Consequently, the near field is significantly enhanced by the hybrid structure of silver nanoparticles and PhC.

2.5. Experimental Verification

Furthermore, in order to experimentally illustrate the enhancement of SERS signal from plasmonic staining by PhC, we compared the Raman signals from silver stained IOPHB and silver stained nonporous hydrogel beads (**Figure 5**). When the staining time is 15 min, the SERS intensities from nonporous hydrogel are very weak, which are about 1/5 of those from the plasmonic stained IOPHB (calculated on peaks intensities at 1542 and 1587 cm^{-1}). Therefore, the staining time of nonporous hydrogel was extended to 6 h to get remarkable Raman signals (blue line, Figure 5a). It is obvious that the average Raman intensity obtained from silver stained

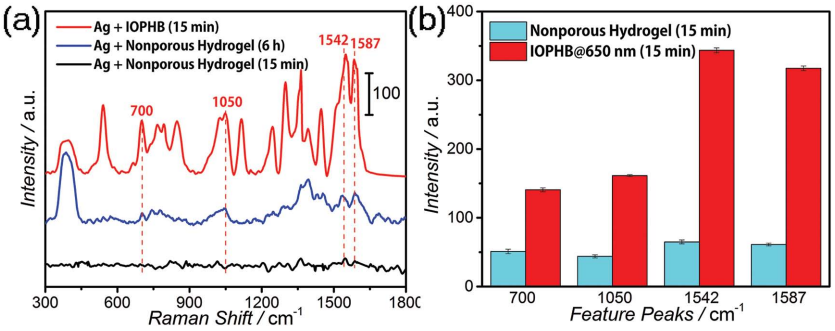

Figure 5. a) Raman spectra of Mb from silver stained IOPHB (15 min, red curve) and silver stained nonporous hydrogel (6 h for blue curve and 15 min for black curve). Spectra were vertically shifted for clarity. b) An average enhancement of 423% was obtained from the comparison between nonporous hydrogel and IOPHB, which was summarized from SERS intensities at four feature peaks.

IOPHB were higher than those from nonporous hydrogel beads. The intensities of Raman peaks at 1542 and 1587 cm^{-1} were increased by about three times when the staining time of the nonporous hydrogel was extended to 6 h. Between IOPHB (15 min stained) and nonporous hydrogel (15 min stained), the enhancement of intensities of Mb feature peaks at 700, 1050, 1542, and 1587 cm^{-1} is 2.75–5.19, averaged to 4.23 (Figure 5b). In general, the SERS intensity could be regarded as proportional to the density of plasmonic nanoparticles. The distribution of silver nanoparticles on the surface of nonporous hydrogels is shown in Figure S4a (Supporting Information). In comparison, the density of silver nanoparticles within IOPHB stained for 15 min is 29.5% larger than that on the surface of nonporous hydrogels stained for 6 h (Figure S4b, Supporting Information). Therefore, there is an extra fourfold increase, which could attribute to the PhC structure of the hydrogel and demonstrated the advantage of the hybridization of plasmonic staining and photonic crystal.

2.6. Multiplexed Protein Analysis

Generally, during the detection of protein by SERS, the protein solution will be mixed with silver sols and then dried so that the sample is concentrated and much more "hot spots" are utilized to increase the sensitivity.[26–28] Thus, the proteins are prone to denature and it is hard to distinguish the proteins from each other in the mixture. In addition, the dry process will result in big analysis variation. However, in our method, the whole process of detection is in solution. No drying procedure is needed and the semiwater phase of the hydrogel will reserve the protein in its native status to the most. As a demonstration, Mb, Cyt C, and Hb, which are three important chromoproteins in human body, were analyzed by IOPHB and plasmonic staining in a multiplexed way. **Figure 6**a–f is the Raman spectra of three main chromoproteins, Mb, Cyt C, and Hb, with different concentrations and SERS intensities of three feature peaks of each protein versus different concentrations for quantitative analysis, respectively. The lowest measurable concentration of Mb, Cyt C, and Hb were 2.73×10^{-3}, 450.5×10^{-6}, and 7.75×10^{-6} M, respectively.

Usually, proteins sharing the same chromophore are difficult to be distinguished using their Raman spectra because some vibrational bands may overlap.[29] Thus, the raw SERS data require further analysis to differentiate proteins. Here, principal component analysis (PCA) was applied to the collected Raman spectra in order to extract the selective feature of original data depending on variance criteria and visualize the extracted features. SERS spectra were obtained from IOPHBs functionalized by three different capture antibodies and exposing them to binary (Mb and Cyt C) and ternary (Mb, Cyt C, and Hb) protein solution mixtures (Figure S5, Supporting Information). The results of PCA show a clear separation in the clusters of the quintuple measurement of above binary and ternary protein mixtures (Figure 6g–i). Principal components of the PCA plots are over 95%, which is beyond the standard of 85%. Thus, the proposed photonic crystal hydrogel based on plasmonic staining is specific and sensitive,capable of distinguishing similar proteins, which also demonstrated its capability of multiplexed detection and provided a new label-free method for protein analysis.

3. Conclusion

In conclusion, inverse opal PhC hydrogel enhanced plasmonic staining was developed for SERS analysis of multiple proteins. Excited by a laser at 532 nm, the PhC hydrogel with its bandgap centered at 650 nm exhibited the best analytic results, in terms of Raman signal strength, RSD and SNR. The plasmonic staining of 3D PhC provides high-density SERS hot spots and meanwhile enhances the interaction of light with plasmonic nanoparticles. These effects benefit the Raman analysis of proteins. Moreover, the hybrid structure is capable of analyzing proteins in a label-free and facile fashion. As an example, three hemeproteins (Mb, Cyt C, and Hb) with the same chromophore component were chosen for multiplexed analysis. Applying the multivariate analysis to the measured Raman spectra can precisely differentiate proteins in binary and ternary mixtures. The strong interaction of light and the hybrid 3D nanostructure of silver nanoparticles and highly ordered inverse opal hydrogel offer new insights into plasmonic nanoparticles and provides experimental and theoretical references for biosensor design and other applications like electrophoresis and chromatography. Thus, this method will benefit the sensing of biomolecules or even microorganisms and will enable widespread applications in life science researches, clinic applications, and food safety monitoring.

4. Experimental Section

Materials: Photonic crystal beads (PCBs) were fabricated with the microfluidic technique developed by our group.[30] Acrylamide,

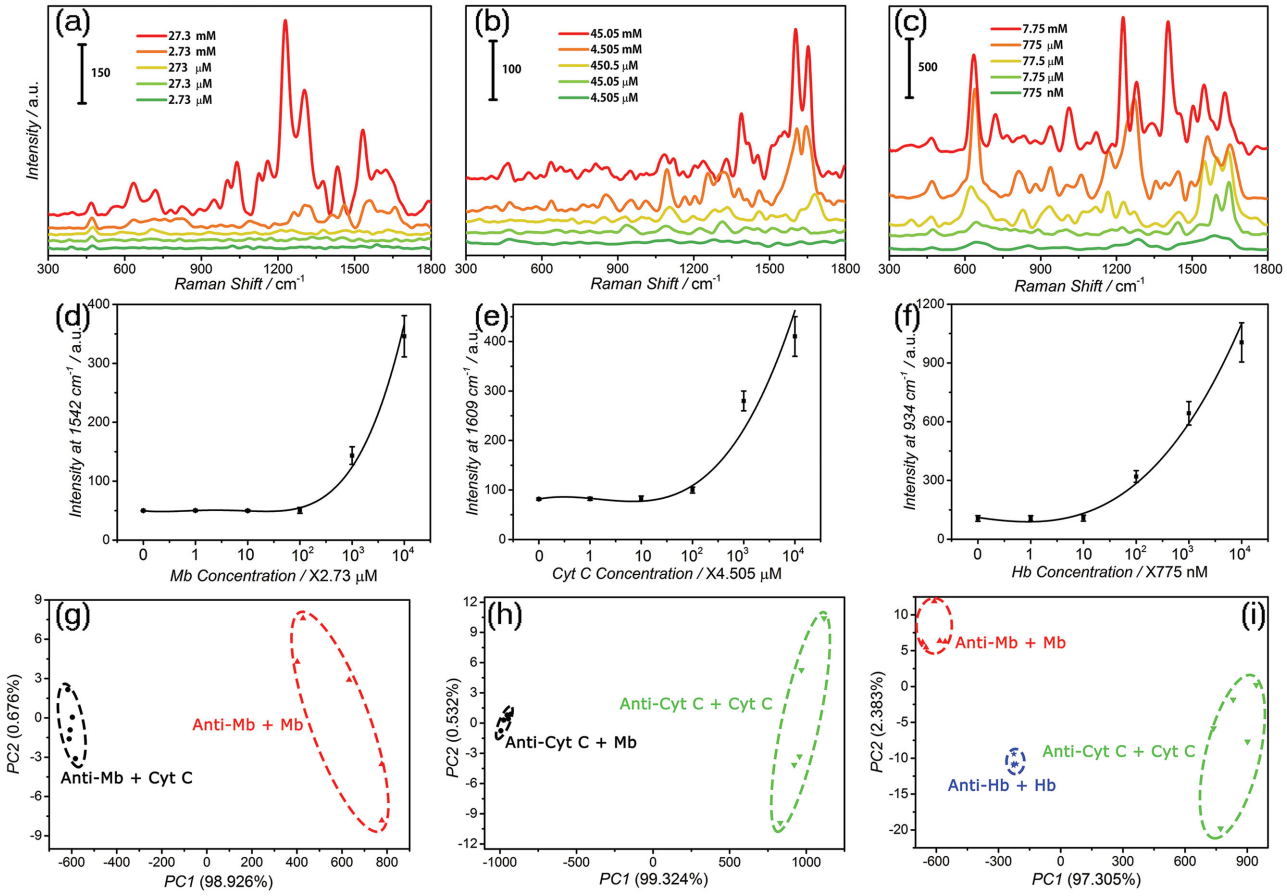

Figure 6. Multiplexed protein analysis. a–c) Raman spectra of Mb a), Cyt C b), and Hb c) with different concentrations. d,e) SERS intensities of feature peaks (1542, 1609, and 934 cm^{-1}) versus different concentrations of Mb d), Cyt C e), and Hb f) (five data averaged). g,h) Principle component analysis (PCA) of Mb and Cyt C binary mixture solution based on Raman spectra. i) PCA of ternary mixture solution of three proteins based on Raman spectra.

bisacrylamide, 2-hydroxy-2-methylpropiophenone (HMPP), and glutaraldehyde were purchased from Aladdin Reagent Company (Shanghai, China). Mouse myoglobin (Mb), rabbit antimouse myoglobin antibody, mouse hemoglobin, rabbit antimouse hemoglobin antibody, mouse cytochrome c, and rabbit antimouse cytochrome c antibody were purchased from Uscn Life Science Inc. (Wuhan, China). All solvents and reagents were of analytical grade and used without further purification. Phosphate buffered saline PBS (pH = 7.4) was used throughout the experiments.

Synthesis of Silver Nanoparticles and Fabrication of IOPHB: Silver sol was synthesized according to the literature.[31] Briefly, a 50 mL glycerol–water mixture (40 vol% glycerol) was stirred and heated up to 95 °C. Then, 9 mg silver nitrate was added to the solvent. One minute later, 1 mL sodium citrate (3%) was added to the solvent. The mixture was kept stirring for 1 h at 95 °C. The fresh prepared silver sol was kept at 4 °C.

Fabrication of PhC hydrogel was described by our previous work.[32] Briefly, 17.4 g acrylamide and 2.6 g bisacrylamide were added to 80 mL double distilled water to make a pregel solution. PCBs with the diameter of about 200 μm were dispersed into the pregel solution and HMPP mixture (100:1.5, v/v) for 2 h. The pregel solution containing the PCBs was subsequently cured under UV light for 30 s. The polymerized hydrogel was incubated in 4 °C ethanol and 60 °C water solution alternately in order to remove the PCBs from the cured hydrogel. Silica templates were removed by 1% HF.

Protein Immobilization in IOPHB and Silver Staining: The protein binding process was shown in Figure S1 (Supporting Information). Briefly, the IOPHB were immerged in 5% (w/w) aqueous solution of glutaraldehyde solution for 4 h. After washed with double distilled water three times, the beads were immerged in 200 μg mL^{-1} antibodies of PBS solution at 4 °C overnight. Then the antibody conjugated beads were blocked by 1% bovine serum albumin to prevent nonspecific binding. Consequently, the beads were incubated in different concentrations of proteins at 37 °C for 1 h. Redundant proteins were washed away with PBS three times. Consequently, the protein conjugated beads were soaked in the freshly prepared silver sol for 5 min to 6 h. The PAM inverse opal beads were washed three times to remove redundant silver nanoparticles.

For multiplexed protein analysis, both anti-Mb and anti-Cyt C conjugated IOPHB were incubated in Mb, Cyt C, Mb and Cyt C mixture solutions alternately and the concentrations are 4.505×10^{-3}, 2.73×10^{-3}, 4.505×10^{-3}, and 2.73×10^{-3} M, respectively.

Device Characterization: A field emission scanning electron microscope (Zeiss Ultra Plus, Germany) was used to obtain the morphology of hydrogel beads. TEM imaging silver nanoparticles and cross section of silver staining IOPHB was performed on a JEM2100EX platform. All SERS signals were collected by a Raman spectrometer (Invia microRaman, Renishaw Inc) with a 50× objective lens throughout the SERS experiments. SERS spectra of

small NANO MICRO

proteins were collected at room temperature with power of 1 mW and exposure time of 10 s. All experiments were performed three times and the spectra data were averaged for each sample unless specified. Reflection spectra of IOPHBs were recorded by an optical microscope (BX51, Olympus) with a fiber-optic spectrometer (USB2000-FLG, Ocean Optics) coupled through a C mount with a customized fiber adaptor.

Simulations: The FDTD simulation was performed using a commercial software (FDTD Solutions, Lumerical Inc.). In the simulation, the computation domain consisted of 24 layers of inverse ovals stacked along the *z*-direction and an array of 2 × 2 ovals in the *x*–*y* plane. The computation domain was truncated by the periodic boundary condition in the horizontal directions (*x*–*y* plane) and the absorbing boundary condition in *z*-direction. The refractive indices of ovals and hydrogel were 1.33 and 1.55, respectively. Lattice constant of the hydrogel crystal and diameter of silver nanoparticles were 323 and 30 nm, respectively. The excitation light illuminated the PhC hydrogel structure from the *z*-direction. The near field distributions were calculated and plotted at 161.5, 161.5, and 323 nm as shown in Figure 4.

Supporting Information

Supporting Information is available from the Wiley Online Library or from the author.

Acknowledgements

Z.M. and X.Z. contributed equally to this work. This paper was supported by National Natural Science Foundation of China (Grant Nos. 21073033, 21373046, and 21327902), Jiangsu Science and Technology Department (Grant No. 2014707), Suzhou Science and Technology Project (Grant No. ZXG2013036), the State Key Lab of Space Medicine Fundamentals and Application (SMFA12K11), Program Sponsored for Scientific Innovation Research of College Graduate in Jangsu Province (CXZZ13_0126) supported by Fundamental Research Funds for the Central Universities, the Program for New Century Excellent Talents in University, and the research Fund for the Doctoral Program of Higher Education of China (20120092130006).

[1] G. Lu, H. De Keersmaecker, L. Su, B. Kenens, S. Rocha, E. Fron, C. Chen, P. Van Dorpe, H. Mizuno, J. Hofkens, J. A. Hutchison, H. Uji-i, *Adv. Mater.* **2014**, *26*, 30.
[2] A. Huefner, W. L. Kuan, R. A. Barker, S. Mahajan, *Nano Lett.* **2013**, *13*, 6.
[3] M. Okada, N. I. Smith, A. F. Palonpon, H. Endo, S. Kawata, M. Sodeoka, K. Fujita, *Proc. Natl. Acad. Sci. USA* **2012**, *109*, 28.
[4] P. M. Kosaka, V. Pini, J. J. Ruz, R. A. da Silva, M. U. Gonzalez, D. Ramos, M. Calleja, J. Tamayo, *Nat. Nanotechnol.* **2014**, *9*, 12.
[5] H. Im, H. Shao, Y. I. Park, V. M. Peterson, C. M. Castro, R. Weissleder, H. Lee, *Nat. Biotechnol.* **2014**, *32*, 5.
[6] S. R. Panikkanvalappil, M. A. Mackey, M. A. El-Sayed, *J. Am. Chem. Soc.* **2013**, *135*, 12.
[7] E. Droghetti, F. P. Nicoletti, L. Guandalini, G. Bartolucci, G. Smulevich, *J. Raman Spectrosc.* **2013**, *44*, 10.
[8] H. Ping, M. Zhang, H. Li, S. Li, Q. Chen, C. Sun, T. Zhang, *Food Control* **2012**, *23*, 1.
[9] M. Kahraman, B. N. Balz, S. Wachsmann-Hogiu, *Analyst* **2013**, *138*, 10.
[10] W. Shen, M. Li, B. Wang, J. Liu, Z. Li, L. Jiang, Y. Song, *J. Mater. Chem.* **2012**, *22*, 16.
[11] G. Lu, H. Li, S. Wu, P. Chen, H. Zhang, *Nanoscale* **2012**, *4*, 3.
[12] M. Chevallet, S. Luche, T. Rabilloud, *Nat. Protoc.* **2006**, *1*, 4.
[13] N. A. V. Neuhoff, D. Taube, W. Ehrhardt, *Electrophoresis* **1988**, *9*, 6.
[14] O. A. Schwint, M. Labraga, C. O. Cervino, M. Haffar, P. H. Sequeiros, H. J. A. Marcos, *Cardiovasc. Pathol.* **2004**, *13*, 185.
[15] Y. C. Cao, R. Jin, C. A. Mirkin, *Science* **2002**, *297*, 5586.
[16] Y. C. Cao, R. Jin, J.-M. Nam, C. S. Thaxton, C. A. Mirkin, *J. Am. Chem. Soc.* **2003**, *125*, 48.
[17] J. F. Li, Y. F. Huang, Y. Ding, Z. L. Yang, S. B. Li, X. S. Zhou, F. R. Fan, W. Zhang, Z. Y. Zhou, Y. Wu de, B. Ren, Z. L. Wang, Z. Q. Tian, *Nature* **2010**, *464*, 7287.
[18] W. Z. Seok-min Kim, B. T. Cunningham, *Opt. Express* **2010**, *18*, 5.
[19] S. Guddala, S. A. Kamanoor, A. Chiappini, M. Ferrari, N. R. Desai, *J. Appl. Phys.* **2012**, *112*, 8.
[20] S. Schlucker, *Angew. Chem. Int. Ed.* **2014**, *53*, 19.
[21] J. D. Joannopoulos, S. G. Johnson, J. N. Winn, R. D. Meade, *Photonic Crystals: Molding the Flow of Light*, 2nd ed., Princeton University Press, Princeton, **2011**.
[22] A. Susanto, T. Herrmann, E. von Lieres, J. Hubbuch, *J. Chromatogr. A* **2007**, *1149*, 2.
[23] M. Heinemann, T. Wagner, B. Doumèche, M. Ansorge-Schumacher, J. Büchs, *Biotechnol. Lett.* **2002**, *24*, 10.
[24] D. W. Mayo, F. A. Miller, R. W. Hannah, *Course Notes on the Interpretation of Infrared and Raman Spectra*, Wiley, Hoboken, **2004**.
[25] S. Schlücker, W. Kiefer, *Surface Enhanced Raman Spectroscopy: Analytical, Biophysical and Life Science Applications*, Wiley, Weinheim, **2013**.
[26] X. X. Han, H. Y. Jia, Y. F. Wang, Z. C. Lu, C. X. Wang, W. Q. Xu, B. Zhao, Y. Ozaki, *Anal. Chem.* **2008**, *80*, 8.
[27] T. Bhuvana, G. V. P. Kumar, G. U. Kulkarni, C. Narayana, *J. Phys. Chem. C* **2007**, *111*, 18.
[28] S. Keskin, M. Culha, *Analyst* **2012**, *137*, 11.
[29] Z. Zhou, X. Han, G. G. Huang, Y. Ozaki, *J. Raman Spectrosc.* **2012**, *43*, 6.
[30] Y. Zhao, X. Zhao, C. Sun, J. Li, R. Zhu, Z. Gu, *Anal. Chem.* **2008**, *80*, 5.
[31] D. Steinigeweg, S. Schlucker, *Chem. Commun.* **2012**, *48*, 69.
[32] Y. J. Zhao, X. W. Zhao, J. Hu, J. Li, W. Y. Xu, Z. Z. Gu, *Angew. Chem. Int. Ed.* **2009**, *48*, 40.

Received: June 24, 2015
Revised: August 5, 2015
Published online: October 5, 2015

